Model for charged dust expansion across a magnetic field

H. Fu and W. A. Scales

Citation: Physics of Plasmas (1994-present) **20**, 073704 (2013); doi: 10.1063/1.4816700
View online: http://dx.doi.org/10.1063/1.4816700
View Table of Contents: http://scitation.aip.org/content/aip/journal/pop/20/7?ver=pdfcov
Published by the AIP Publishing

PHYSICS OF PLASMAS **20**, 073704 (2013)

Model for charged dust expansion across a magnetic field

H. Fu[1,2] and W. A. Scales[1]
[1]*Bradley Department of Electrical and Computer Engineering, Virginia Polytechnic Institute and State University, Blacksburg, Virginia 24061, USA*
[2]*Key Laboratory of Wave Scattering and Remote Sensing Information and School of Information Science and Technology, Fudan University, Shanghai 200433, China*

(Received 25 May 2013; accepted 24 June 2013; published online 24 July 2013)

Plasma fluctuations arise in the boundary region between charged dust clouds and background plasmas. A self-consistent computational model is developed to study expansion of a charged dust cloud across a magnetic field, creation of the inhomogeneous boundary layer and associated processes. The charging of the dust particulates produces a boundary layer and associated ambipolar electric field. This ambipolar field provides a source for low frequency dust acoustic waves in unmagnetized plasmas. A background magnetic field if sufficiently strong, may impact the dust acoustic wave evolution and dust density structures due to $\mathbf{E} \times \mathbf{B}$ and diamagnetic current generation. The dust acoustic density fluctuation generation across a strong magnetic field ($\omega_{pe}/\Omega_{ce} \ll 1$) may be suppressed as compared to an unmagnetized dusty plasma, which will be discussed. Fluctuations generated at longer timescales propagating along the dust boundary layer will also be investigated in the lower hybrid and dust lower hybrid frequency range. Applications to space and laboratory plasmas are discussed. © *2013 AIP Publishing LLC*. [http://dx.doi.org/10.1063/1.4816700]

I. INTRODUCTION

When dust cloud particulates exist spatially localized in a plasma background, the dust particles start to charge up by accumulating background plasma. The charging process may cause a plasma density depletion region. A gradient in the density of charged plasma species arises at the edge of the dust cloud boundary layer, where an ambipolar electric field develops. The ambipolar electric field in the dust cloud boundary layer provides an energy source for exciting plasma waves. The presentence of a background magnetic field may alter plasma fluctuation generation by impacting the coupling between the plasma dynamics and the charged dust particulates.[1,2]

In unmagnetized dusty plasmas, dust acoustic waves have been investigated and reported.[3–7] The conditions for exciting dust acoustic waves in collisionless dusty plasmas were first obtained by Rosenberg,[8] who showed that the dust acoustic wave can be driven unstable by ion and electron drifts greater than the dust acoustic phase speed. The dust acoustic wave in an unmagnetized boundary layer plasma could possibly be generated due to electron flow above the dust acoustic phase speed across the boundary in space applications.[9] In laboratory dusty plasma experiments, the large amplitude self-excited dust acoustic waves were considered to be generated by streaming ions and electrons with velocity of the order of the ion acoustic speed along the magnetic field.[10–12] Nevertheless, self-excited dust acoustic wave generation has been attributed to the electric field.

The existence of a background magnetic field prevents the charged particles from freely streaming perpendicular to the magnetic field. Apart from EIC modes[13] in a magnetized dusty plasma, the cross-field dust acoustic instability in a inhomogeneous dust boundary layer may behave quite differently from unmagnetized dusty plasmas particularly when electrons are strongly magnetized. The dust acoustic turbulence may possibly generate diffusion of the order of the ion thermal speed across the boundary layer. The dust cloud expansion across the magnetic field may produce conditions for generating waves along the boundary layer in the lower hybrid frequency range through a shear-driven instability[14–16] and the lower-hybrid drift instability.[17–19] The shear-driven instability in expanding dust clouds has been studied by computational simulations with massless fluid electrons and fluid ions on ion timescales in previous works.[20–22] Plasma fluctuations in the lower hybrid frequency/dust lower hybrid frequency range due to $\mathbf{E} \times \mathbf{B}$ flow and diamagnetic drifts will be investigated by the new model in this work on longer dust timescales.

In this paper, a two-dimensional hybrid model has been developed to investigate possible plasma instabilities in charged dust cloud boundary layers in magnetized dusty plasmas. A charging model is adopted to deal with particle current collection in the dust charging process. The dust acoustic instability produced in a boundary layer will be investigated in both an unmagnetized and magnetized plasma. The excitation mechanism for such dust waves in a magnetized dusty plasma will be discussed in this work. Finally, important features of possible lower hybrid type instabilities will also be described. The paper is organized as following. In Sec. II, a computational model is described in detail. Section III describes computational results for the dust acoustic instability across the boundary and plasma instabilities along the boundary. Applications are discussed in Sec. IV and summary is given in Sec. V.

II. COMPUTATIONAL MODEL

In this section, a two-dimensional electrostatic periodic hybrid computational model is described to investigate

plasma instabilities in the plane perpendicular to the geomagnetic field $\mathbf{B} = B_0\hat{z}$. Electrons are described by fluid equations. The continuity equation for electrons is given by

$$\frac{\partial n_e}{\partial t} + \nabla \cdot (n_e \mathbf{v}_e) = \left.\frac{dn_e}{dt}\right|_{\text{charge}} + P_e + L_e, \tag{1}$$

where

$$\left.\frac{dn_e}{dt}\right|_{\text{charge}} = -\frac{1}{q_e}\frac{d\rho_{de}}{dt}. \tag{2}$$

Here, ρ_{de} is the dust charge density due to electron charging current collection. P_e is the production of electrons due to ionization of neutrals, and L_e is the loss of electrons due to recombination with plasma ions. For typical model calculations, $L_e = \kappa n_i n_e$, where κ is the recombination coefficient and P_e may be determined in terms of κ and the equilibrium electron density n_{e0} in the absence of dust.

The momentum equation for electrons perpendicular to the geomagnetic field is

$$\frac{\partial \mathbf{v}_e}{\partial t} + (\mathbf{v}_e \cdot \nabla)\mathbf{v}_e = \frac{q_e}{m_e}(\mathbf{E} + \mathbf{v}_e \times \mathbf{B}) - \frac{k_B T_e}{m_e}\frac{\nabla n_e}{n_e} - \nu_{en}(\mathbf{v}_e - \mathbf{v}_n), \tag{3}$$

where n_α, $\mathbf{v}_\alpha$, T_α are the density, velocity, and temperature of the α charged species and $\alpha = e, i, d$ denotes electrons, ions, and dust, respectively. Here, q_α and m_α are the charge and mass of the α species, and $\mathbf{E}$ and $\mathbf{B}$ are the electric field and magnetic field. $\mathbf{v}_n$ is the neutral gas velocity, k_B is Boltzmann's constant, and ν_{en} is the electron-neutral collision frequency. Equations (1) and (3) are solved spatially with pseudo-spectral methods, and a second-order Adams-Bashfourth-Moulton predictor-corrector scheme is used for the time advance. The full Poisson's equation $\epsilon_0\nabla^2\phi = -(q_e n_e + q_i n_i + q_d n_d)$ was solved by spectral methods, and the electric field was obtained by $\mathbf{E} = -\nabla\phi$, where ϕ is the electrostatic potential and ϵ_0 is the vacuum permittivity.[23]

The dynamics of ions are modeled as discrete particles with the standard Particle-In-Cell PIC method[24] by integrating the Lorentz force equation. The particle ion density loss is

$$\frac{dn_i}{dt} = \left.\frac{dn_i}{dt}\right|_{\text{charge}} + P_i + L_i, \tag{4}$$

where

$$\left.\frac{dn_i}{dt}\right|_{\text{charge}} = -\frac{1}{q_i}\frac{d\rho_{di}}{dt} \tag{5}$$

and ρ_{di} is the dust particle charge density due to ion charging current collection. $P_i = P_e$ is the ion production and $L_i = L_e$ is the ion loss due to recombination, respectively. These production and loss mechanisms are implemented with standard ionization and absorption techniques (e.g., Ref. 26), however, for the present study which will concentrate on generation of dust density fluctuations, they are neglected for simplicity.

A Monte Carlo model is adopted to realize the ion density loss due to dust charging current collection. The probability for removing the j*th* ion particle is $P^j = dn_i^j/n_i^j$, where dn_i^j and n_i^j are the ion density variance and ion density information at the j*th* particle position, which are obtained based on weighted information from neighboring nodes as commonly adopted in PIC method. The probability P^j is calculated from the ion current, which will be stated shortly. An event occurs when a uniformly distributed random number on the interval [0 1] is less than the probability P^j.

The dynamics of dust are modeled as discrete particles with the standard Particle-In-Cell PIC method. The dust particles are assumed to have a uniform mass m_d (although the model allows for mass distributions) and a time variable charge for the jth dust grain particle $Q^j(t) = -Z_d^j e$, where Z_d^j is the charge number on the dust particle and e is the unit electron charge. Electrons and ion currents are collected by a spherical grain. In the condition of the dust grain radius r_d less than the shielding length λ_d, the time dependent charge on the dust can be described by the Orbit Motion Limited OML approach[25]

$$\frac{dQ^j}{dt} = I_e^j + I_i^j + I_p^j, \tag{6}$$

where I_e^j and I_i^j are the electron and ion currents collected by the jth dust grain and I_p^j is the photoemission current. Assuming negatively charged dust, the electron and ion currents on the jth dust grain are given by

$$I_e^j = \sqrt{8\pi} r_d^2 q_e n_e v_e \exp\left[\frac{-q_e\phi_f^j}{k_B T_e}\right], \tag{7}$$

$$I_i^j = \sqrt{8\pi} r_d^2 q_i n_i v_i \left[1 - \frac{q_i\phi_f^j}{k_B T_i}\right]. \tag{8}$$

The photoemission electron current for negative dust grains[32] is

$$I_p^j = -\pi r_d^2 q_e J_p Q_{ab} Y_p. \tag{9}$$

Here, $v_\alpha = \sqrt{k_B T_\alpha/m_\alpha}$ is the thermal velocity and $\phi_f^j = Q^j/C = Q(t)/4\pi\epsilon_0 r_d$ is the floating potential on the dust grain, where C is the grain capacitance. At F-layer peak altitudes for space applications, the dominant plasma ion species is atomic oxygen plasma in the ionosphere. The equilibrium grain surface floating potential ϕ_f is $-3.6k_B T_e/e$ for oxygen plasma and $-2.5k_B T_e/e$ for hydrogen plasma, which is the representative ion of higher altitudes in the ionosphere. The equilibrium dust charge state is given by OML theory as $Z_d \propto r_d|\phi_f/e|$. Also, J_p, Q_{ab}, Y_p, and T_p are the photon flux, photon absorption efficiency, photoelectron yield, and average photoelectron temperature. It is valid to use the standard currents even for a magnetized plasma environment, since the dust radius size r_d (assumed no more than several microns) is much less than the electron cyclotron radius (which is of the order of millimeters).[27]

The photoemission current may be important in the daytime and should be included as above. But it is ignored for present applications in this work. By ignoring the photoemission effect, the electron and ion density reduction is only caused by the dust charging effect. The ion current I_i determines the ion particle reduction probability P^j. The dust

charge density variance due to ion charging current collection is calculated from the ion current at grids using $d\rho_{di} = d(n_d q_d) \simeq n_d I_i dt$. The ion density variance dn_i^j is obtained from the $d\rho_{di}$ through Eq. (6), giving the probability P^j for the ion density reduction. Since this work only focus on the dust grain charging process, other chemical production and loss terms are ignored in this work.

The ion-neutral elastic scattering events are assumed to be hard sphere elastic collisions. A Monte Carlo Collision (MCC) model is used to treat ion and cold neutral collisions.[24,28] The collision probability for the *jth* particle is $P^j = 1 - \exp(-\Delta t \sigma_{in} n_g V_i)$, where V_i, σ_{in}, n_g is the velocity of particle, ion and neutral collision cross-section, and neutral gas density, respectively. A collision occurs when a uniformly distribution random number on the interval [0 1] is less than the collision probability P^j. Other MCC collision methods to deal with plasma particles and neutrals can be considered with multi-step collision.[29]

In this model, electron and ion densities are taken to be uniform initially. The profile of the dust cloud density is considered in the form

$$n_d = n_{d0}\left[\tanh\left(\frac{x - x_1}{w}\right) - \tanh\left(\frac{x - x_2}{w}\right)\right], \qquad (10)$$

where n_{d0} is the unperturbed density of uncharged dust, x_1 and x_2 are the location of the right and left boundary of dust cloud, respectively, and w is the scale length of the boundary. Dust particles are assumed to charge negatively to the equilibrium potential and have uniform dust radius and mass. The dust-neutral collisions can damp out the dust acoustic waves for highly collisionality as shown in Ref. 9 using a one-dimensional Langevin dust-neutral model.

III. SIMULATION PARAMETERS AND RESULTS

In this model, the electron and ion density are initialized with equal unperturbed background density $n_{i0} = n_{e0}$. The dust density relative to background plasma density may vary with time depending on applications as shown in Table I. An important application is for ionospheric modification experiments.[30] Plasma parameters at the altitude ~280 km are typically as follows. The dominant ion species is O^+, $m_i/m_e = 16 \times 1836, n_{e0} = n_{i0} = 3 \times 10^{11}\,m^{-3}, T_e = T_i = 0.1\,eV,$ and $B = 0.5\,G$. The ion Debye length is $\lambda_{di} \sim 0.4\,cm$ in the unperturbed plasma and the ion plasma frequency is $\omega_{pi} \sim 1.8 \times 10^5\,rad/s$. The dust charging time is roughly estimated based on $\tau_c = \omega_{pi}^{-1}(\lambda_d/r_d)$, using $T_d = 0.1\,eV$.[31,32] The charging time is ~0.005 s for a dust grain of radius $r_d = 4\,\mu m$, which corresponds to the equilibrium charge number $Z_{d0} = 1000$. The charging time is ~0.02 s for $r_d = 1\,\mu m$, which corresponds to the equilibrium charge number $Z_{d0} = 250$. The dust plasma frequency ω_{pd} is ~52.6 rad/s for the dust mass $m_d = 10^{10} m_i$, the dust density $n_d = 0.00085 n_e$, and the dust charge number $Z_d = 1000$. The dust time scale is estimated to be ~0.019 s, while the ion time scale is $\sim 5.5 \times 10^{-6}$ s. The dust charging time is therefore approximately on the order of the dust time scale.

TABLE I. Parameters for a magnetized charged dust cloud.

Parameters	Ionospheric[31,38]	Laboratory[2]
Plasma density ($n_e \sim n_i$)	$3 \times 10^{11}\,m^{-3}$	$10^{16}\,m^{-3}$
Electron temperature (T_e)	0.1 eV	3 eV
Ion temperature T_i	0.1 eV	0.025 eV
Ion species	O^+	Ar^+
Dust species	Al_2O_3 spheroid	silica microparticle
Dust radius (r_d)	$0.1 - 10\,\mu m$	$0.25 - 5\,\mu m$
Dust charge number (Z_d)	25–2500	800–10 000

All quantities in the simulation are normalized to the ion initial quantities. Lengths are normalized to the ion Debye length, temperature to the initial ion temperature, frequencies or time to the initial ion plasma frequency, and velocities to the initial ion thermal velocity. In the simulation, the simulation domain has $L_x = 1024\lambda_d$ with 1024 grid cells and $L_y = 256\lambda_d$ with 256 grid cells with periodic boundary conditions in both dimensions. In each grid cell $dx = dy = \lambda_d$, there are 25 particles for each species (i.e., ions and dust), respectively. The initially uncharged dust cloud occupies about $256\lambda_d \times 256\lambda_d$ with a prescribed boundary scale length. The cloud is centered in the simulation domain, which implies $x_1 = 384\lambda_d$ and $x_2 = 640\lambda_d$. Fig. 1 shows a schematic representation of the dust boundary layer simulation sketching the profile of electron density, the ambipolar electric field, and dust density with an initial scale length $w = 5.12\lambda_d$. The ambipolar electric field rises on the edge of the boundary layer and becomes stronger with a sharp gradient.

To make the simulation feasible, we choose the ion and electron mass ratio $m_i/m_e = 1836$ for H^+ and the dust and ion mass ratio $\sim m_d/m_i = 10^5$ to include the dust inertia in the simulation without loss of generality.[33] Results are qualitatively consistent with cases for atomic hydrogen H^+ and atomic oxygen O^+. The ratio of the dust plasma frequency to the ion plasma frequency ω_{pd}/ω_{pi} is 0.092 in the simulation. The time step is chosen to be $\omega_{pi}\Delta t = 0.004$ in order to insure adequate energy conservation and low noise level in the simulation.

Two sets of instabilities are considered including dust acoustic instability across the boundary and instabilities due to electron cross flow along the boundary. The dust acoustic instability may arise from plasma flow across the dust

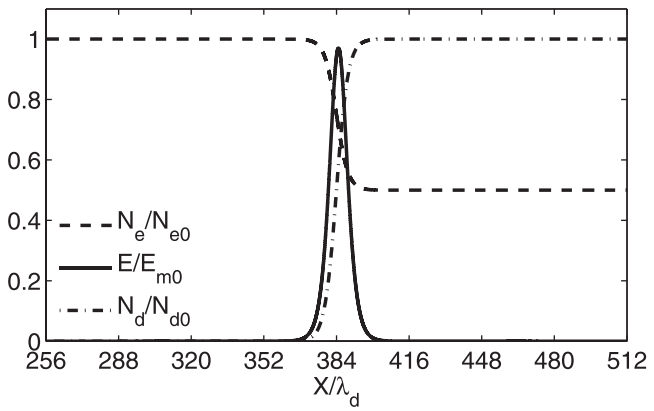

FIG. 1. Schematic representation of the boundary layer problem. Note that the E_m is the peak value of the electric field.

boundary in the $\hat{x}$ direction. On one hand, one scenario is that if the dust is relatively cold, the initialed localized dust cloud determines the plasma density gradient. The charging time scale determines the plasma density depletion percentage. The time scale of the dust acoustic instability is impacted not only by the ambipolar electric field evolution but also the dust inertial scale. In strongly magnetized dusty plasmas, the dust expansion speed is important for driving the dust acoustic wave and the lower hybrid instability. The dust expansion speed may serve as a precondition for exciting the lower-hybrid instability in this scenario. On the other hand, another scenario when the dust is hot and thermalized initially, the lower hybrid instability can develop once the electron cross flow develops.

A. Dust acoustic instability

In this section, dust acoustic waves are considered in both unmagnetized dusty plasmas and magnetized dusty plasmas with the dust temperature $T_d = T_e = T_i$. The magnetic field strength on the evolution of the dust acoustic instability is considered. The ratio ω_{pe}/Ω_{ce} is varied by changing the magnetic field amplitude only. The time evolution of the total electrostatic field energy is shown in Fig. 2 for $\omega_{pe}/\Omega_{ce} \to \infty (B = 0)$ and $\omega_{pe}/\Omega_{ce} = 0.35$ with electron-neutral collision frequency $\nu_{en}/\omega_{pi} = 0.1$. The electric field energy is calculated by $\frac{1}{2}\int |\mathbf{E}|^2 dxdy$. The electrostatic field energy primarily grows in the $\hat{x}$ direction, which is the density gradient direction across the boundary layer. One of the features observed is that the time to obtain the maximum electrostatic energy reduces as the magnetic field is increased. The required time continues to decrease further as the frequency ratio ω_{pe}/Ω_{ce} reduces. Results indicate that if $\omega_{pe}/\Omega_{ce} \gg 1$, the field energy develops similarly as the unmagnetized case. The maximum electrostatic field energy saturates at a high level by increasing the magnetic field. The maximum electrostatic field energy is attributed to the charge separation in the density gradient $\hat{x}$ direction due to different confinement of the electrons, ions and dust as well as charge separation due to the development of any instability.

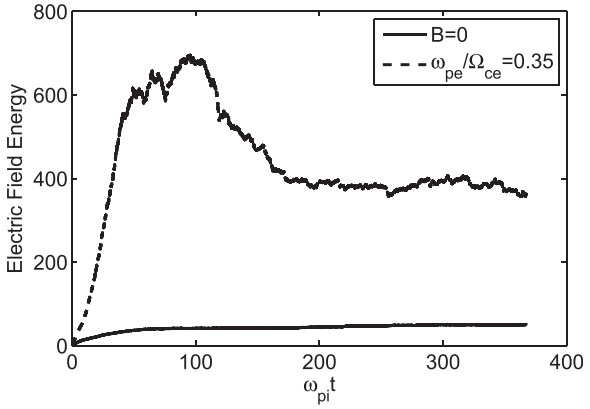

FIG. 2. Time evolution of the electrostatic field energy (normalized) for two cases $\omega_{pe}/\Omega_{ce} \to \infty (B = 0)$ and $\omega_{pe}/\Omega_{ce} = 0.35$ with electron-neutral collision frequency $\nu_{en}/\omega_{pi} = 0.1$.

1. For the unmagnetized case B = 0 or $\omega_{pe}/\Omega_{ce} \gg 1$

In an unmagnetized dusty plasma, for the dust acoustic wave in the regime $\omega \gg kv_d$, the dust acoustic wave frequency is given by

$$\omega = kc_D/(1 + k^2\lambda_d^2)^{1/2}, \tag{11}$$

where $c_D = \omega_{pd}\lambda_d$ is the dust acoustic speed and $\lambda_d = \lambda_{de}\lambda_{di}/\sqrt{\lambda_{de}^2 + \lambda_{di}^2}$. For a dusty plasma with negatively charged dust grains, we have $\lambda_d \simeq \lambda_{di}$. In the long wavelength $k^2\lambda_d^2 \ll 1$, the dust acoustic frequency is $\omega = kc_D$.[5] The wavelength of the dust acoustic wave is of the order $\sim 10\lambda_{di}$ in the simulation. The frequency power spectrum of the electric field in the $\hat{x}$ direction for the dust acoustic wave is approximately maximized near the dust plasma frequency. Using these parameters, the dust acoustic phase velocity in the simulation is $v_p = \omega/k \simeq 0.5\omega_{pd}/k_x = 0.092v_i$, which agrees with the dust acoustic phase speed approximately given by $c_{DA} = Z_{d0}v_i(n_{d0}/n_{i0})^{1/2}(m_i/m_d)^{1/2} = 0.092v_i$ in the long-wavelength limit $k^2\lambda_d^2 \ll 1$.[32]

Fig. 3 depicts a one-dimensional X cross-section of electron density n_e/n_{e0}, ion density n_i/n_{i0}, dust density n_d/n_{d0}, and the density difference $(n_e - n_i + n_dZ_d)/n_0$, and the ambipolar electric field E_x/E_0 in the top panel and electron flow velocity V_{ex}/v_i, ion flow velocity V_{ix}/v_i, and dust flow velocity V_{dx}/v_i for $\omega_{pe}/\Omega_{ce} \to \infty (B = 0)$ with the electron-neutral collision $\nu_{en}/\omega_{pi} = 0.1$. The electric field component is normalized by $E_0 = k_B T_e/e\lambda_{Di}$. In general, when the dust starts to charge negatively, the electron density depletion region starts to form, while the ion density depletion percentage is relatively small because of lower mobility. It is noted that the maximum electric field corresponds to where the

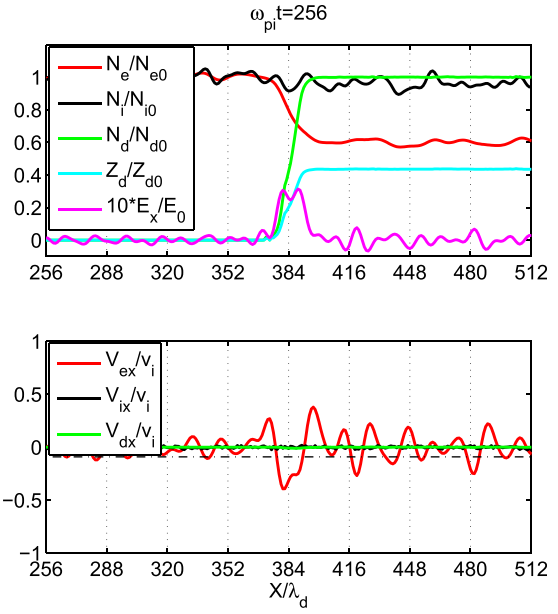

FIG. 3. One-dimensional X cross-section of electron density, ion density, dust density, dust charge number density, the density difference, electric field (top) and the electron flow velocity, ion flow velocity and the dust flow velocity for $\omega_{pe}/\Omega_{ce} \to \infty (B = 0)$. Note that the dust acoustic phase speed(-dash-dot line) $c_{DA} = 0.092v_i$.

total plasma density profile changes sign based on Gauss' law. The wave electric field to the first order charge densities is $\partial E/\partial x = (e/\epsilon_0)(n_i - n_e - n_d Z_d)$. The resulting charge separation gives rise to an electric field pointing towards the center of the dust cloud. The maximum electric fields correspond to the maximum negative electron flow velocity in the $\hat{x}$ direction before waves develop. The dust density inhomogeneity provides the ambipolar field as the energy source for exciting instabilities. For Boltzmann behavior for the electrons, the electric field in the $\hat{x}$ direction is approximately $E_x \approx (k_B T_e/q_e)(\partial \log n_e/\partial x)$.[34] The electron drift flow velocity in the $\hat{x}$ direction is approximately given by $V_{ex} = q_e E_x/m_e \nu_{en}$ in an unmagnetized plasma. The electron drift relative to ions and dust grains is considered to be the energy source for exciting dust density fluctuations in unmagnetized dusty plasmas as shown in Fig. 3.

When waves start to develop, the electron flow velocity $V_{ex} = 0.5 v_i$ exceeds the dust acoustic phase speed $c_{DA} = 0.092 v_i$ as shown in Fig. 3. At this time $\omega_{pi} t = 256$, there is no apparent net ion flow and dust flow simultaneously in the boundary. The dust density fluctuations start to develop initially at the point, where the ambipolar field is the maximum and then propagate inwards as will be shown later. In unmagnetized dusty plasmas, at a later time, the electron fluctuation shows anticorrelation relation relative to the dust fluctuation in the simulation. The mechanism for exciting the dust acoustic wave is possibly the electron flow velocity driven by sufficiently large electric field in unmagnetized dusty plasmas, which agrees with work in an alternate one-dimensional model.[9,34] The linear analysis described in Ref. 9 shows that the threshold for exciting the dust acoustic instability is the electron flow velocity above the dust acoustic phase speed in unmagnetized dusty plasmas. Based on linear analysis, it is observed that the maximum wave growth rate is of the order $0.001\omega_{pd}$ and the wave frequency is of the order of ω_{pd}. A spectrum of wavenumbers could be unstable with the maximum wave growth rate near $k_x \lambda_d < 1$.

2. For the case $\omega_{pe}/\Omega_{ce} \ll 1$

In a strongly magnetized dusty plasma environment, the magnetic field can be sufficiently strong to make both electrons and ions magnetized. Most importantly, the magnetic fields confine electrons moving across the magnetic field and correspondingly may impact the electron density fluctuation level. Although the magnetic field strength if sufficiently strong can also make ions magnetized particularly for a long time scale, we focus on analysis if electrons are magnetized assuming $\omega_{pe}/\Omega_{ce} \ll 1$.

Fig. 4 shows a one-dimensional X cross-section plot of electron density n_e/n_{e0}, ion density n_i/n_{i0}, dust density n_d/n_{d0}, and the density difference $(n_e - n_i + n_d Z_d)/n_0$, the electric field E_x/E_0 and the electron, ion, and dust flow velocity for $\omega_{pe}/\Omega_{ce} = 0.35$ with electron-neutral collision frequency $\nu_{en}/\omega_{pi} = 0.1$ at time $\omega_{pi} t = 88$. This time corresponds to that when the dust acoustic wave starts to develop. The maximum amplitude of the ambipolar electric field becomes stronger in comparison to the unmagnetized case in Fig. 3. The electric field E_x becomes stronger while the

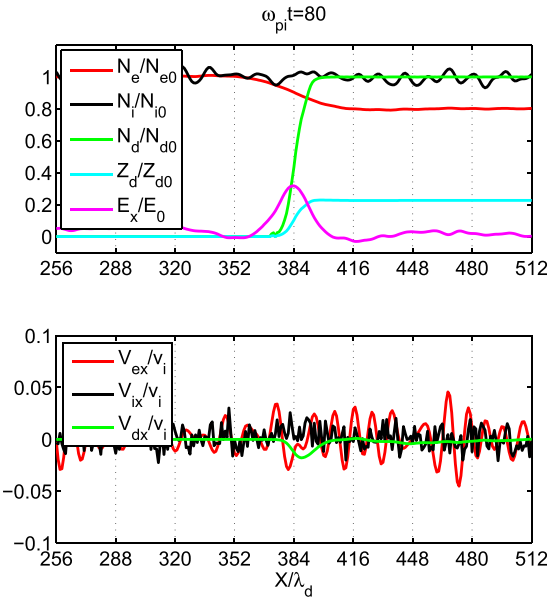

FIG. 4. One-dimensional X cross-section of electron density, ion density, dust density, dust charge number density, the density difference, electric field (top), and the electron flow velocity, ion flow velocity, and the dust flow velocity for $\omega_{pe}/\Omega_{ce} = 0.35$.

electron flow velocity V_{ex} in the $\hat{x}$ direction becomes smaller, simply using the perpendicular electron flow velocity approximately $V_{ex} = E_y/B_0 + (k_B T_e/eB_0 n_e)(\partial n_e/\partial y)$ without considering electron inertia and collision effects. The density fluctuation level in plasma densities at the wave linear growth stage is suppressed if the frequency ratio ω_{pe}/Ω_{ce} further reduces.

The electron flow velocity threshold drops to $V_{ex}/v_i = 0.05$, which is below the dust acoustic sound speed for the strongly magnetized case $\omega_{pe}/\Omega_{ce} = 0.35$ with $\nu_{en}/\omega_{pi} = 0.1$. For a even smaller ratio $\omega_{pe}/\Omega_{ce} < 0.2$, there is no substantial net electron and ion flow along the $\hat{x}$ direction, but a dust drift velocity could be observed as shown in Fig. 4. When both electrons and ions are unable to traverse across the magnetic field, we propose that the strong electric field may drive the dust flow velocity relative to electron and ions, which may possibly provide the energy source for exciting dust acoustic waves. Therefore, with the magnetic field, the dust acoustic wave can be excited easily but the dust density fluctuation level may become relatively weak.

Fig. 5 shows a two-dimensional plot of dust density n_d/n_{d0} at three different times $\omega_{pi} t = 112$, 160, 336. At early linear time stage $\omega_{pi} t = 112$, the dust acoustic density fluctuations start to be observed, and propagate towards the dust boundary layer center[9] as compared to that at time $\omega_{pi} t = 160$. The fluctuation structures are observed in both the dust density and the dust charge number. As the dust acoustic wave develops, such dust density wave structures in the boundary layer will lead to diffusion of dust clouds across the magnetic fields such as at a later time $\omega_{pi} t = 336$. The outward diffusion modifies the sharpness of the dust boundary layer. If the ambipolar electric field is sufficiently large, the dust acoustic wave may exhibit nonlinear structures. For a strongly magnetized case, the dust acoustic instability results in a fast diffusion rate of the dust clouds across

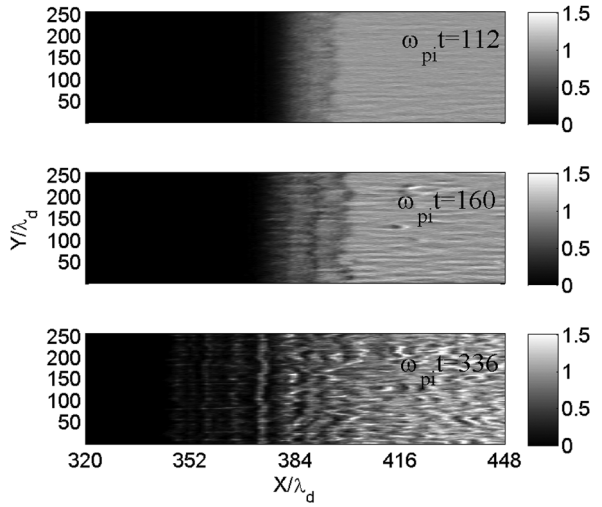

FIG. 5. Two-dimensional dust density structures n_d/n_{d0} at different times for a strongly magnetized case. Note that the dust acoustic wave initially propagates inwards the dust cloud at early times and then diffuses outwards.

the magnetic field. The resulting dust diffusion velocity could be a portion of the ion thermal velocity. The dust acoustic wave development contributes to the dust cloud layer expansion that leads to the formation of a negatively charged dust drift beam as a potential important factor for exciting instabilities in the $\hat{y}$ direction.

In summary, the magnetic field plays an important role on the ambipolar electric field as well as the evolution of the dust acoustic waves. Importantly, the excitation mechanism for the dust acoustic waves in a magnetized dusty plasma may be distinguished from the unmagnetized dusty plasma. The transition of strongly magnetized electrons to weakly magnetized electrons could be achieved through varying the magnetic field amplitude and correspondingly the ratio ω_{pe}/Ω_{ce}. As the magnetic field strengthens, the ambipolar electric field increases while the electron fluctuation due to dust acoustic waves becomes less prominent. The dust density fluctuation can still exist and become weak, while the magnetic field amplitude is sufficiently large to impact the electrons and ions in the plasma.

Another important factor impacting electron dynamics and correspondingly the dust acoustic wave excitation is the electron-neutral collision effect. Depending on different applications, Fig. 6 shows the electron-neutral collision

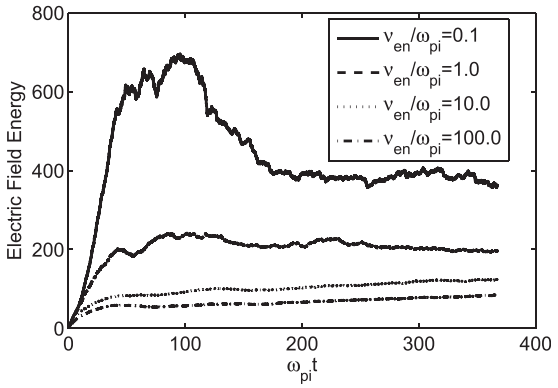

FIG. 6. The electron-neutral collision effect on the field energy development for $\omega_{pe}/\Omega_{ce} = 0.35$.

effects on the electric field energy for $\omega_{pe}/\Omega_{ce} = 0.35$. The electron-neutral collision frequency is assumed constant during the dust charging process. With electron-neutral collisions, the electrons could move across the boundary perpendicular to the geomagnetic field. Once electrons can move freely with $\nu_{en}/\omega_{pi} \gg 1$, the dust acoustic wave generation mechanism for strongly magnetized electrons reduces to that for unmagnetized electron dynamics. The electron-neutral collisions weaken the maximum ambipolar electric field amplitude and enhance the electron diffusion in the boundary layer region across a magnetic field.

B. Instabilities due to electron cross flow

Plasma instabilities could be driven by the cross-field flows in the presentence of inhomogeneities in densities. The localized dust clouds charge up to form a localized electron density depletion region, where instabilities can arise along the boundary region in the $\hat{y}$ direction. The energy sources for exciting plasma instabilities along the boundary include a $\nabla n \times \mathbf{B}$ density gradient drift, $\mathbf{E} \times \mathbf{B}$ electric drift, the nonuniformity of the density gradient, and the electric field as sketched in Fig. 7. Neglecting electron inertia, the electron drift perpendicular to the magnetic field $\mathbf{B} = B_0\hat{z}$ is

$$V_{ey} = V_E + V_{de}, \tag{12}$$

where $V_E = -E_x/B_0$ is the equilibrium $\mathbf{E} \times \mathbf{B}$ drift velocity, and $V_{de} = (k_B T_e/eB_0 n_e)(\partial n_e/\partial x)$ is the diamagnetic drift velocity. The ion velocity in the perpendicular plane neglecting ion density gradient is approximately

$$V_{iy} = V_E. \tag{13}$$

In this part, the first section investigates the lower-hybrid shear-driven instability due to sheared $\mathbf{E} \times \mathbf{B}$ flow[22] by starting from a late time initial condition with prescribed density gradients and thermalized dust for computational efficiency. A diffusive cloud expansion $T_d \gg T_i = T_e$ is chosen to include the expansion speed for thermalized dust. The fundamental features of lower-hybrid shear-driven instability

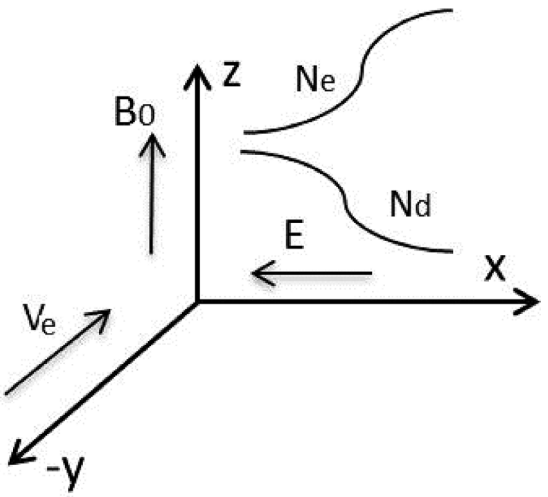

FIG. 7. Schematic of the slab model geometry for $\mathbf{E} \times \mathbf{B}$ flow and diamagnetic electron flow.

will be investigated in greater detail and on longer timescales than past works utilizing the new model. The second section will study plasma instabilities along the boundary for $T_d = T_i = T_e$ using a self-consistent model. Without assuming diffusive dust expansion and prescribed plasma density depletion condition, the dust density depletion region develops due to the dust grain charging process while the dust diffusion arises from the ambipolar electric field and the dust acoustic instability self-consistently. The resulting dust thermal expansion speed across the magnetic fields may provide a condition to stimulate dust lower-hybrid drift instability along the boundary in a dust cloud boundary layer.

1. High frequency lower-hybrid shear-driven instability

This section provides a feasible and efficient methodology to study fundamental features of high frequency lower hybrid shear-driven density structures using the new model in order to compare fluctuations that may be also observed in a boundary layer independently. This model includes the electron inertia, electron-neutral collisions, ion kinetic effects, and magnetized ions compared to previous models. The scenario provides useful instability analysis for applications to dust boundary layer problems with relatively high dust density and large dust particles producing steep density gradients. As discussed in previous works,[20–22] this instability in a diffusively expanding dusty plasma may be important for active space modification experiments.

A diffusively expanding dusty plasma cloud is initially established with the dust thermal speed $v_d = 0.3v_i$ by including the dust dynamics. The heavier thermal dust with much larger gyroradii is unmagnetized at early times, and attempt to stream outward. The resulting charge separation produces an electric field pointing outwards from the dust cloud, leading the magnetized electrons to undergo an $\mathbf{E} \times \mathbf{B}$ electron flow in the $\hat{y}$ direction. The electric field is nonuniform leading to a shear in the electron drift, so both the electron-ion relative drift and the shear provide sources of free energy. At a time scale of the order of several ion gyroperiods, the relative electron-ion drift velocity becomes relatively weak without collisions; the shear flow provides the major sources of free energy and possibilities for vortex formation.

The shear frequency generated by the density gradient is defined $\omega_S = V_{E0}/L_E$, where V_{E0} is the peak electron flow velocity and $L_E = V_E/(dV_E/dx)$ represents the flow's shear scale length. The lower hybrid frequency is $\omega_{LH} = \omega_{pi}/\sqrt{1+\omega_{pe}^2/\Omega_{ce}^2}$. Reference 15 shows that a sheared electron cross-field flow excites the electron-ion-hybrid EIH shear-driven instability if $\kappa = \omega_S/\omega_{LH} > 1$ and coherent structures longer than the electron gyro radius; for $\kappa = \omega_S/\omega_{LH} < 1$ the lower-hybrid drift instability dominates with short wavelength near the order of the electron gyro radius[18] and there is no vortex formation. The scale length of the electron flow is generally considered in the range $\rho_e < L_E < \rho_i$ to excite lower hybrid shear-driven instability,[16] which is the initial dust cloud boundary condition for our previous dust acoustic wave simulations. For this case, the shear frequency is comparable to the lower hybrid wave frequency. The scale length of the inhomogeneities to excite lower-hybrid drift instability can be many ion Larmor radii. These instabilities due to electron cross flow are high frequency in the range of the lower hybrid frequency ω_{LH} compared to the dust plasma frequency ω_{pd}.

The mechanism for the EIH instability perpendicular to the magnetic field is the electron flow velocity V_{ey}. The local dispersion relation in frequency ω and wavenumber k_y for this instability has been described previously[22,36]

$$\tilde{\omega}^4 + \left(\frac{\delta_i}{\tilde{k}_y}S - \frac{\alpha_i}{\delta_i}\tilde{k}_y\right)\tilde{\omega}^3 - \tilde{\omega}^2 + \frac{\alpha_i}{\delta_i}\tilde{k}_y\tilde{\omega} = 0, \qquad (14)$$

where $\tilde{\omega} = \omega/\omega_{LH}$, $\tilde{k}_y = k_y L_E$, $\delta_i = \omega_{pi}/\Omega_{ci}$, $S = L_E/L_N$, and $\alpha_i = V_{ey}/\Omega_{ci}L_E$, where V_{ey} is the electron drift flow velocity along the boundary and $L_N = n_e/(dn_e/dx)$ is the electron density gradient scale length. This EIH shear-driven instability generates turbulence in the range of lower hybrid frequency ω_{LH}. The wave growth rate $\gamma \leq \omega_{LH}$ maximized at $k_y L_E \sim 1$. The wavelength of the waves is determined by the gradient scale length L_E of the electron flow V_E as shown in several references.[21,22]

Fig. 8 shows the time evolution of the electric field energy for a typical simulation case $\omega_{pe}/\Omega_{ce} = 0.15$ without any collisions. The ambipolar electric field in the density gradient $\hat{x}$ direction grows initially and hence the resulting highly sheared $\mathbf{E} \times \mathbf{B}$ electron flow provides free energy for the development of shear-driven lower-hybrid waves along the boundary in the $\hat{y}$ direction. Subsequently, the electric field E_y grows in a lower hybrid time scale due to the development of the EIH instability. The shear waves oscillate around the lower hybrid wave frequency. The simulation lower-hybrid shear wave frequency is calculated based on the frequency power spectrum of wave signatures such as the electric field E_y at the boundary layer region. A large portion of the power is concentrated around the lower hybrid wave frequency. The waves grow and saturate in several lower hybrid periods, with a rough estimation of the wave growth rate $\gamma/\omega_{LH} \sim 0.1$ in the simulation. Fluctuations grow in electron density in the $\hat{y}$ direction initially and then saturate when vortex structure starts to develop in electron dynamics.

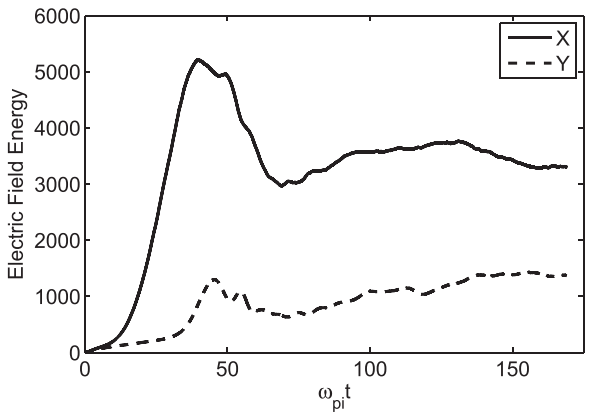

FIG. 8. Time evolution of the electrostatic field energy for EIH instability for the ratio $\omega_{pe}/\Omega_{ce} = 0.15$.

Fig. 9 shows a one-dimensional X cross-section plot of electron density n_e/n_{e0}, ion density n_i/n_{i0}, dust density n_d/n_{d0}, the electron flow velocity V_{ey}/v_i, and two dimensional electron density structures at two different times $\omega_{pi}t = 40$ and $\omega_{pi}t = 56$ for the ratio $\omega_{pe}/\omega_{ce} = 0.15$. Waves start to grow linearly and then saturate. At a linear stage $\omega_{pi}t = 40$, the maximum electron flow velocity reaches up to a value $V_{ey}/v_i = 10$. The mode number $m_y = 8$ is observed in plasma density structure in the $\hat{y}$ direction at a linear stage, which corresponds to a wavelength $\lambda = 32\lambda_d$. The electric field profile could be expressed as $E(x) = (E_0/N_0)\{F(\varsigma - x_0) - F(\varsigma + x_0)\}$, where $\varsigma = x - L_x/2, F(\zeta) = \sec h^2(\zeta/L_E), N_0 = 1 - \sec h^2(2x_0/L_E)$.[15] Note that L_E is the characteristic length over the electron flow, satisfying $\rho_e < L_E < \rho_i$. For a given characteristic length $L_E = 5.12\lambda_d$, the simulation wavelength $\lambda = 32\lambda_d$ is in close accordance with the fastest growing mode as derived from linear theory that $k_y L_E \sim 1$. When waves become saturated at a time $\omega_{pi}t = 56$, vortex structures start to develop. The shear-driven instability produces the vortex-like structure of the order of the velocity shear scale size.

Fig. 10 shows a two-dimensional plot of electron density n_e/n_{e0}, ion density n_i/n_{i0}, dust density n_d/n_{d0}, and the dust charge number Z_d/Z_{d0} for $\omega_{pe}/\Omega_{ce} = 0.15$ at a late time. At a later time $\omega_{pi}t = 164$, fluctuation structures in the $\hat{y}$ direction are observed in the electron density, ion density structure as well as dust density, and dust charge number. The fluctuation initially appears in the electron density, and then cause fluctuations in ion density, dust density as well as dust charge number correspondingly after a long time period. The nonlinear vortex for the EIH instability can cause the transverse ion acceleration[35] as well as dust acceleration.[20] Nonlinear wave structures in electron density are clearly observed, this instability if formed may have strong impact on ground-based radar signals for space applications. It should also be noted that in a longer time scale when the scale size of the electron flow broadens larger than the ion gyro radius, the ions become magnetized, and conditions may be satisfied for cascading toward lower frequency and longer wavelength.[35]

The excitation of shear-driven instability depends on the boundary condition, magnetic fields, the dust parameters as well as collision effects. Moreover, it is critical to observe that in a longer time scale which includes dust dynamics, the

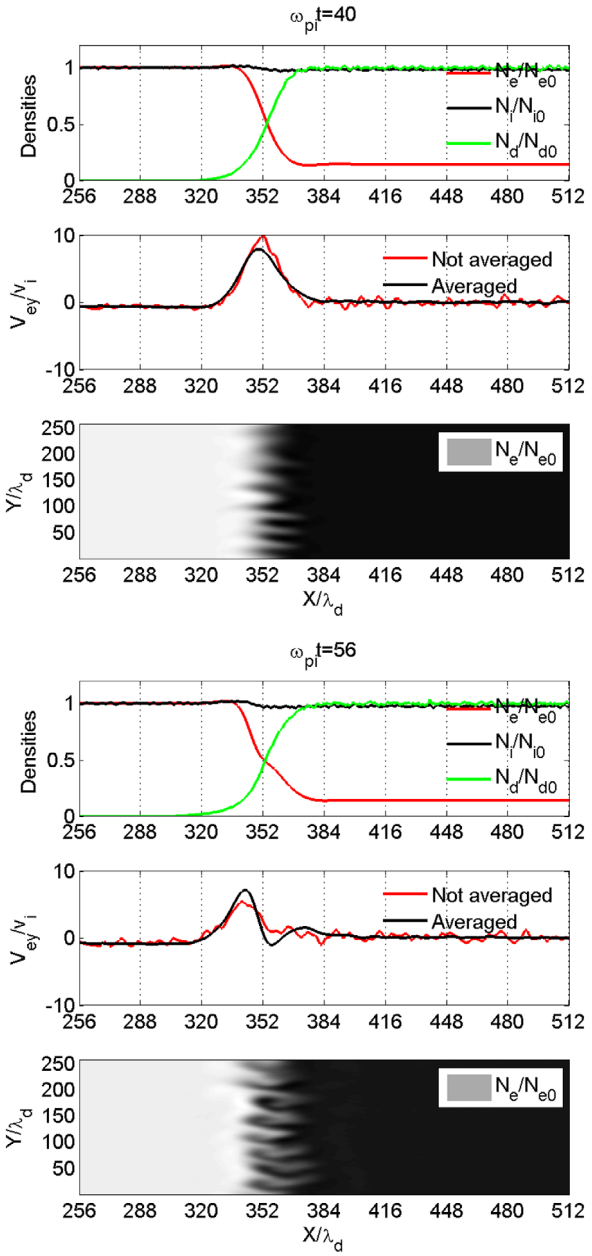

FIG. 9. One-dimensional plot of densities, electron flow in the y direction and two-dimensional electron structures at two different times $\omega_{pi}t = 40$ and $\omega_{pi}t = 56$ for the ratio $\omega_{pe}/\Omega_{ce} = 0.15$.

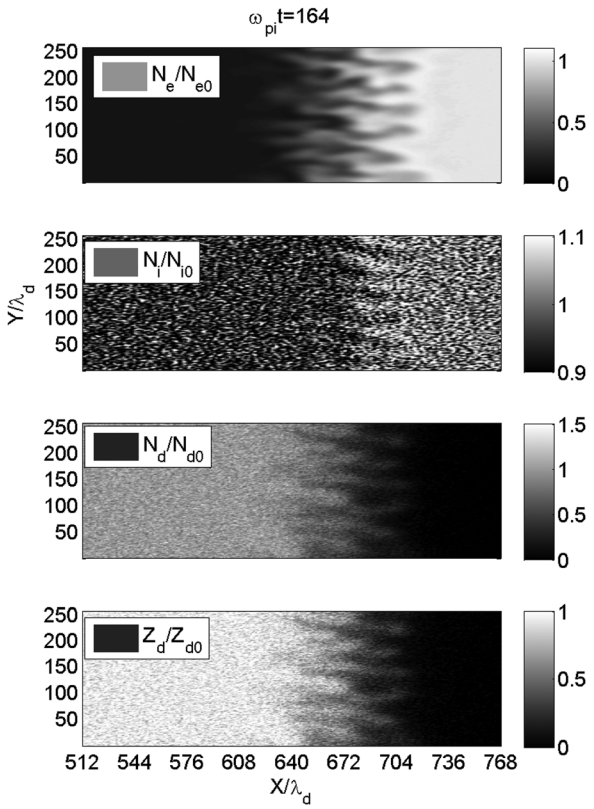

FIG. 10. Two-dimensional plot of electron density, ion density, dust density, and dust charge number density at time $\omega_{pi}t = 164$ for the ratio $\omega_{pe}/\Omega_{ce} = 0.15$.

EIH shear-driven instability can also drive the dust density fluctuations, which have been ignored for all previous works.

2. Low-frequency drift instability

With prescribed plasma density depletion, the previous section considers a sharp dust cloud boundary $\rho_e < L_E < \rho_i$ for a relatively high dust density and large dust grain particles using diffusively expanding dust clouds if $T_d \gg T_e = T_i$. The section considers self-consistent plasma density depletion creation due to the dust charging process and the dust expansion as well as the low-frequency instability in the dust plasma frequency range for $T_d = T_e = T_i$. Compared to the high frequency EIH shear-driven instability, the low-frequency drift instability occurs at a relatively late time after the dust acoustic instability of the previous section develops. The dust grains start from a neutralized state and then charge by accumulating plasma electrons and ions. During this process, a particular focus will be on the structures along the boundary in the $\hat{y}$ direction using the self-consistent model in comparison to the previous lower-hybrid shear instability.

The electrostatic field energy evolution is shown in Fig. 11 for the case $\omega_{pe}/\Omega_{ce} = 0.15$ with electron-neutral collision frequency $\nu_{en}/\omega_{pi} = 1.0$. The ambipolar electric field E_x develops and grows as shown in the expanded plot of the field energy in Fig. 11(top). In a time scale larger than the ion gyro-time scale and approximately the dust plasma time scale, since ions become magnetized and cannot move freely, the electric field reaches a first maximum. Afterwards, the inward directed ambipolar electric field continues to increase before the cold dust starts to move. It is noted that the ambipolar field is in the opposite direction to that for the diffusively expanding dust clouds. The ambipolar electric field reaches a maximum at approximately $\omega_{pi}t \geq 68$ when dust acoustic fluctuations start to develop as described in the first section. At a late time $\omega_{pi}t > 700$, the field energy in the $\hat{y}$ direction starts to grow, which indicates fluctuations generated from a secondary mechanism as will be described in this section.

Fig. 12 shows a one-dimensional X cross-section plot of electron density n_e/n_{e0}, ion density n_i/n_{i0}, dust density

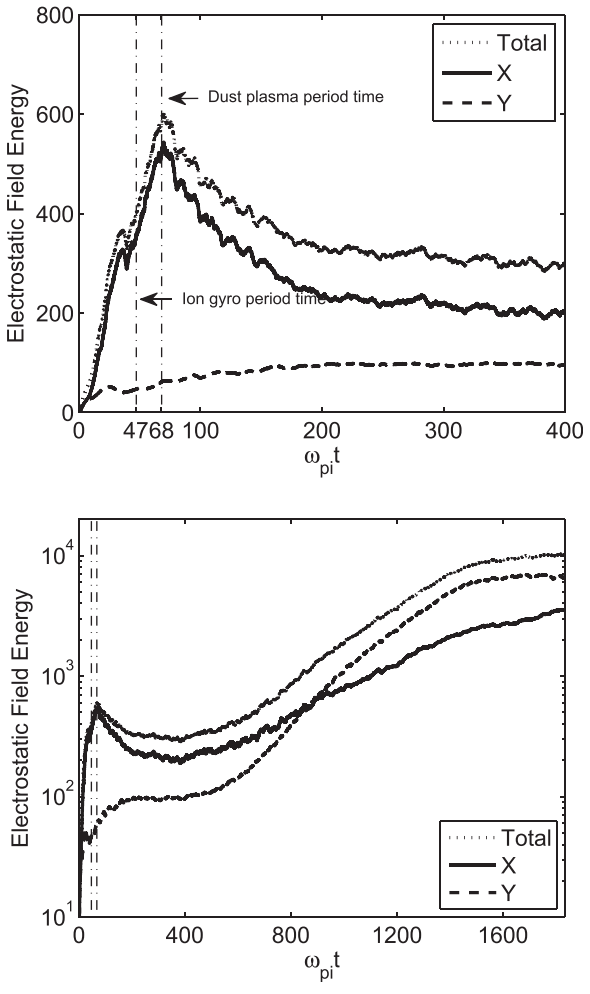

FIG. 11. Time evolution for the electrostatic field energy (normalized) for $\omega_{pe}/\Omega_{ce} = 0.15$ with electron-neutral collision frequency $\nu_{en}/\omega_{pi} = 1.0$.

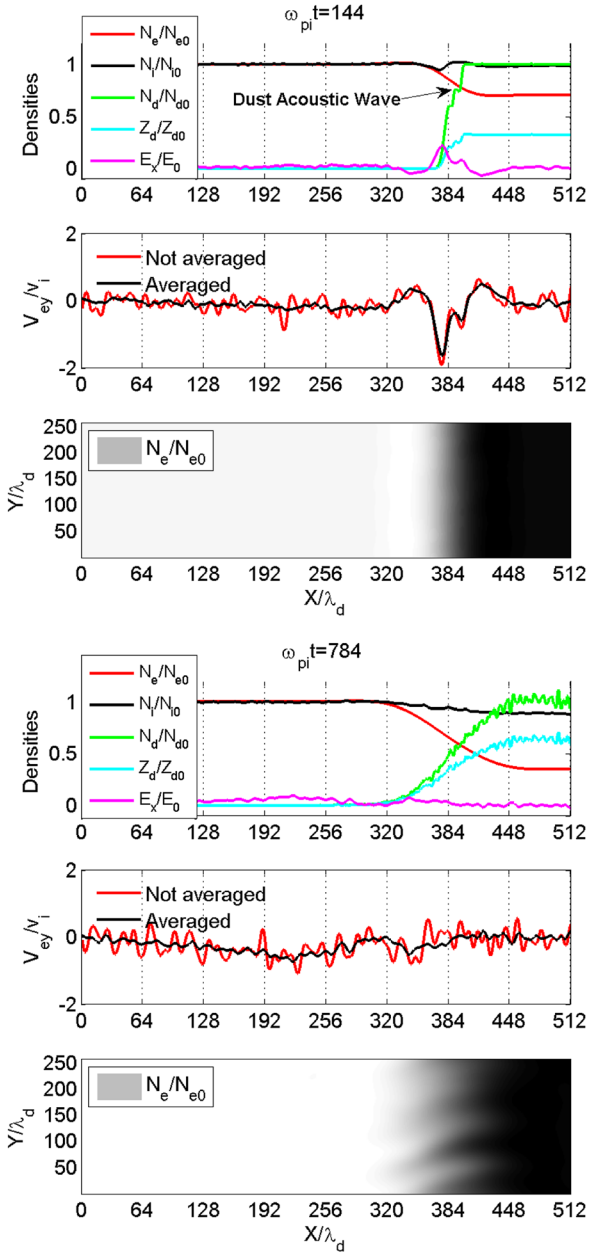

FIG. 12. One-dimensional plot of densities, electron flow in the y direction, and two dimensional electron structures at two different times $\omega_{pi} = 144$ and $\omega_{pi} = 784$.

n_d/n_{d0}, the electric field E_x/E_0(top panel), the electron flow velocity V_{ey}/v_i (middle panel), and two-dimensional electron density structures (bottom panel) at two different times $\omega_{pi}t = 144$ and $\omega_{pi}t = 784$. The dust acoustic fluctuations occur in the dust density along the $\hat{x}$ direction at time $\omega_{pi}t = 144$ in the top panel and fluctuations in electron density in the $\hat{y}$ direction occur at a time $\omega_{pi}t = 784$ in the bottom panel. The dust acoustic waves start to develop structures in dust density and correspondingly the electric field and the electron flow velocity. The fluctuations in the electron density are rather weak to observe particularly for a strongly magnetized case. It is noted that electron cross flow V_{ey} at $\omega_{pi}t = 144$ is in opposite direction to the diffusively expanding dust clouds case for the lower-hybrid shear-driven instability as show in Fig. 9. The dust acoustic structures cause the dust to diffuse outwards and thermalize dust particles. The electron fluctuations are observed clearly in the $\hat{y}$ direction in the boundary layer region at a late time $\omega_{pi}t = 784$. The wavelength of this instability is corresponding to a shallower boundary layer compared to previous shear-driven instability. These electron structures in Fig. 12(b) propagate in the positive $\hat{y}$ direction similarly as the lower-hybrid shear-driven case. The power spectrum of wave frequency is maximized about $\omega \simeq (0.3 \sim 0.5)\omega_{pd} \ll \omega_{LH}$ according to the power spectrum of the electric field E_y, and the wave growth rate is roughly estimated to be $\gamma \simeq 0.03\omega_{pd}$. These fluctuations are considered to be caused by the density gradient.

This instability with a lower frequency compared to the lower-hybrid EIH shear-driven instability is considered to be a dust lower-hybrid drift type instability. The density gradient driven instability resonates with the dust lower-hybrid wave. As a rough estimation, the wave frequency of the dust lower-hybrid drift instability[37] is approximately given by $\omega/\omega_{DLH} = (1 + \sqrt{3}i/2)R^{1/6}$, where $R = (V_E/\Omega_{ce}L_N)^{1/6}(\omega_{pe}^2/\omega_{pd}^2)^{1/6}$ and the dust lower-hybrid (DLH) wave frequency is $\omega_{DLH} = \omega_{pd}/\sqrt{S_2}$ with $S_2 = 1 + \omega_{pe}^2/\Omega_{ce}^2 + \omega_{pi}^2/\Omega_{ci}^2$. Using $V_E/v_i = 0.5$ and $L_N = 64\lambda_d$, the wave frequency is estimated approximately $\omega \simeq 0.10\omega_{pd}$ and the maximum wave growth rate is $\gamma \simeq 0.1\omega_{pd}$. The wavelength about $\sim 85\lambda_d$ at time $\omega_{pi}t = 784$ in the simulation is in reasonable agreement with linear analysis $kV_E \approx R^{1/2}\omega_{DLH}$.[37] It should be noted that the electron flow threshold for this instability is quite smaller than that for the lower-hybrid shear-driven instability in the previous section. Also, the boundary sharpness in this section exists in a regime that $\rho_e < \rho_i < L_E$, when electron drift wave interacts with a dust lower hybrid wave. Fig. 13 shows a two-dimensional plot of electron density n_e/n_{e0}, ion density n_i/n_{i0}, dust density n_d/n_{d0}, and the dust charge number Z_d/Z_{d0} for $\omega_{pe}/\Omega_{ce} = 0.15$ at a late time. At time $\omega_{pi}t = 896$, fluctuation structures in the $\hat{y}$ direction are observed in the electron density, ion density structure as well as dust density and dust charge number. The flute modes are observed for this low frequency instability without vortex structures as observed for the shear-driven instability. These low frequency plasma waves occur at a long period, when the scale size of densities becomes greater than the ion gyro radius for both magnetized electrons and ions. No obvious vortex structures are observed for this instability.

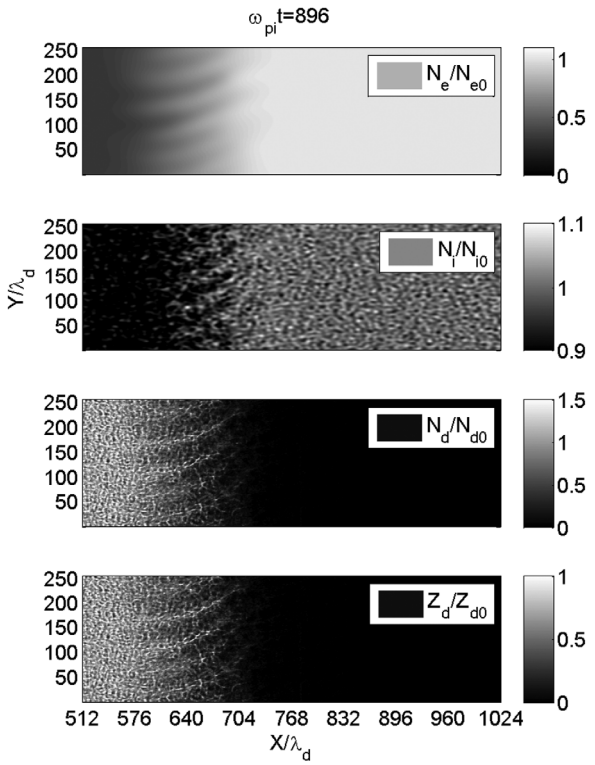

FIG. 13. Two-dimensional plot of electron density, ion density, dust density, and dust charge number density at time $\omega_{pi}t = 896$.

IV. DISCUSSION OF APPLICATIONS

Such similar boundary layer problems could occur in various cases such as the polar mesosphere region, active space ionospheric and magnetospheric modification experiments, and laboratory dusty plasmas.[3,30,38–41] This model could also be extended to study phenomena related to boundary layer effects in a conventional plasma environment.

One application will involve dusty boundary layer problems in the space environment. Such plasma processes may be observed with ground-based radars and *in-situ* space instruments. For the charged aerosol release experiment(CARE),[30] the gradient of the dust cloud edge and the sharpness of electron density gradient are important factors to determine the turbulence in a boundary layer. The electron density depletion is determined by the dust parameters such as dust density, dust particle size, and the dust charging process. A sharp electron density gradient will be favorable for exciting these instabilities. On one hand, the dust acoustic wave will possibly occur on the edge of the dust cloud, which propagates towards the center of the clouds. Also, the dust acoustic turbulence may cause dust heating and anomalous diffusion. It should be pointed out that the dust acoustic wave excitation may be quenched by the dust-neutral collisions as shown in Ref. 9. The dust acoustic instability may be also applied to polar mesospheric summer echoes (PMSEs) regions as discussed. On the other hand, perpendicular to geomagnetic field, the shear-driven instability/lower-hybrid drift instability may also occur along the boundary. It is noted that the shear-driven/lower-hybrid drift instability depends on the magnetic field and the electron density gradient scale significantly. The shear-driven/lower-hybrid drift instability may cause a relative

large electron density fluctuation compared to the electron fluctuation caused by the dust acoustic wave, which will highly depend on the electron density depletion gradient. The shear-driven instability/lower-hybrid drift instability will also cause fluctuations in ion density, dust density, and dust charge number.

Another important application will be in the category of laboratory dusty plasmas. Most laboratory dusty plasma waves have been studied in unmagnetized conditions.[2] New laboratory facilities are under development, which will have the capability to study the role of magnetic fields in dusty(complex) plasma environments.[2] The self-consistent models developed in this work have the capability of describing the dust charging process, unmagnetized and magnetized plasma dynamics and wave excitation in an inhomogeneous magnetized dusty plasma environments. The dust acoustic wave excitation in a strongly magnetized dusty plasma has been discussed in this paper. The excitation for the dust acoustic instability in strongly magnetized dusty plasmas may be distinct from the unmagnetized dusty plasmas. The nonlinear dust acoustic structures may also be impacted by the magnetic fields. Plasma instabilities perpendicular to the magnetic field may also occur along the boundary including the lower-hybrid shear-driven and the dust lower-hybrid drift instability as described in this paper.

V. SUMMARY

A new hybrid two-dimensional computational model has been developed to investigate instabilities in nonuniform magnetized dusty plasmas. The magnetic fields have been applied to study the effect on plasma wave excitation. A charging model has been adopted to deal with the dust grain charging process. A simple but efficient algorithm is adopted to deal with ion current collection in the particle-in-cell method. The dust acoustic instability produced in the boundary layer has been investigated with magnetic field effects. The localized dust clouds produce electron density depletion due to the dust charging process. The ambipolar electric field provides the energy source for exciting the dust acoustic wave and lower- hybrid shear-driven/dust lower-hybrid drift instability. The magnetic field strength impacts both dust acoustic wave instability and lower-hybrid shear-driven/drift instability. The excitation mechanism for such dust acoustic waves in unmagnetized/magnetized dusty plasmas has been compared and discussed. Electron/ion magnetization will play an important role for excitation mechanism, the ambipolar electric field, and dust density fluctuation amplitude perpendicular to the magnetic field. The excitation mechanism for such dust acoustic waves in a strongly magnetized dusty plasma will be most likely due to a dust flow relative to plasma ions and electrons. The dust acoustic wave may cause the dust cloud anomalous diffusion across the magnetic field. The dust cloud expansion leads to a lower-hybrid shear-driven/dust lower-hybrid drift instability in the $\hat{y}$ direction, which can be produced simultaneously with the dust acoustic wave in the $\hat{x}$ direction in the plane perpendicular to the magnetic field.

In this work, this model is mainly used to study possible plasma turbulence during the charged aerosol release experiments in space plasmas. Meanwhile, it also has potential applications for magnetized dusty plasmas for complex plasma research with upcoming experiment facilities.[2] Depending on applications, parameters will be studied thoroughly by including ion-neutral collisions and dust-neutral effects in the future. Nonlinear characteristics may be observed for a large amplitude of dust density fluctuations in a unmagnetized/magnetized dusty plasmas.[7] This model also has the capability to study other instabilities such as electrostatic ion-cyclotron/dust cyclotron waves in magnetized dusty plasmas.[42]

ACKNOWLEDGMENTS

This work was supported by the National Science Foundation grant and the Naval Research Laboratory. The authors would like to appreciate A. Mahmoudian for useful discussions and kind help.

[1]M. Rosenberg and P. K. Shukla, J. Plasma Phys. **70**, 317 (2004).
[2]E. Thomas, Jr., R. L. Merlino, and M. Rosenberg, Plasma Phys. Controlled Fusion **54**, 124034 (2012).
[3]A. Barkan, R. L. Merlino, and N. DAngelo, Phys. Plasmas **2**, 3563 (1995).
[4]V. E. Fortov, A. G. Khrapak, S. A. Khrapak, V. I. Molotkov, A. P. Nefedov, O. F. Petrov, and V. M. Torchinsky, Phys. Plasmas **7**, 1374 (2000).
[5]N. N. Rao, P. K. Shukla, and M. Y. Yu, Planet Space Sci. **38**, 543 (1990).
[6]T. Trottenberg, D. Block, and A. Piel, Phys. Plasmas **13**, 042105 (2006).
[7]R. L. Merlino, J. R. Heinrich, S.-H. Hyun, and J. K. Meyer, Phys. Plasmas **19**, 057301 (2012).
[8]M. Rosenberg, Planet. Space Sci. **41**, 229 (1993).
[9]A. Mahmoudian and W. A. Scales, J. Geophys. Res. **117**, A02304, doi:10.1029/2011JA017204 (2012).
[10]R. L. Merlino, Phys. Plasmas **16**, 124501 (2009).
[11]M. Rosenberg, J. Vac. Sci. Technol. A **14**, 631 (1996).
[12]H. Fu and W. A. Scales, IEEE Trans. Plasma Sci. **40**, 1223 (2012).
[13]N. D'Angelo, Planet. Space Sci. **38**, 1143 (1990).
[14]H. Romero, G. Ganguli, Y. C. Lee, and P. J. Palmadesso, Phys. Fluids B **4**, 1708 (1992).
[15]H. Romero, G. Ganguli, and Y. C. Lee, Phys. Rev. Lett. **69**, 3503 (1992).
[16]H. Romero and G. Ganguli, Phys. Fluids B **5**, 3163 (1993).
[17]R. C. Davidson, N. T. Gladd, C. S. Wu, and J. D. Huba, Phys. Fluids **20**, 301 (1977).
[18]J. F. Drake, P. N. Guzdar, A. B. Hassam, and J. D. Huba, Phys. Fluids **27**, 1148 (1984).
[19]D. Winske, Phys. Fluids B **1**, 1900 (1989).
[20]M. R. Bordikar and W. A. Scales, IEEE Trans. Plasma Sci. **40**, 946 (2012).
[21]G. S. Chae, W. A. Scales, G. Ganguli, P. A. Bernhardt, and M. Lampe, IEEE Trans. Plasma Sci. **28**, 1694 (2000).
[22]W. A. Scales, M. R. Bordikar, A. Mahmoudian, and H. Fu, IEEE Trans. Plasma Sci. **38**, 880 (2010).
[23]H. Fu and W. A. Scales, J. Geophys. Res. **117**, A07317, doi:10.1029/2012JA017704 (2012).
[24]C. K. Birdsall, IEEE Trans. Plasma Sci. **19**, 65 (1991).
[25]I. B. Bernstein and I. N. Rabinowitz, Phys. Fluids **2**, 112 (1959).
[26]C. K. Birdsall and A. B. Langdon, *Plasma Physics via Computer Simulation* (CRC Press, 2005).
[27]L. Patacchini, I. H. Hutchinson, and G. Lapenta, Phys. Plasmas **14**, 062111 (2007).
[28]V. Vahedi and M. Surendra, Comput. Phys. Commun. **87**, 179 (1995).
[29]N. A. Gatsonis, R. E. Erlandson, and C. I. Meng, J. Geophys. Res. **99**(A5), 8479, doi:10.1029/93JA03145 (1994).
[30]P. A. Bernhardt, J. B. Baumgardner, A. N. Bhatt, A. Coster, P. J. Erickson, C. R. Kaplan, R. A. Haaser, M. F. Larsen, F. D. Lind, T. R. Pedersen, R. F. Pfaff, P. A. Roddy, S. P. Rodriquez, P. W. Schuck, C. L.

Siefring, S. M. Smith, E. R. Talaat, and J. F. Thomason, IEEE Trans. Plasma Sci. **40**, 1267 (2012).
[31]M. Rosenberg, P. A. Bernhardt, and S. E. Clark, Planet. Space Sci. **59**, 312–318 (2011).
[32]P. K. Shukla and A. A. Mamun, *Introduction to Dusty Plasma Physics* (Institute of Physics, Bristol, UK, 2002).
[33]D. Winske, S. P. Gary, M. E. Jones, M. Rosenberg, D. A. Mendis, and V. W. Chow, Geophys. Res. Lett. **22**, 2069, doi:10.1029/95GL01983 (1995).
[34]W. A. Scales and G. Ganguli, New J. Phys. **6**, 12 (2004).
[35]G. Ganguli, M. J. Keskinen, H. Romero, R. Heelis, T. Moore, and C. Pollock, J. Geophys. Res. **99**(A5), 8873, doi:10.1029/93JA03181 (1994).
[36]W. A. Scales, P. A. Bernhardt, and G. Ganguli, J. Geophys. Res. **100**(A1), 269, doi:10.1029/94JA02490 (1995).
[37]M. Rosenberg and P. K. Shukla, Plasma Phys. Controlled Fusion **46**, 1807 (2004).
[38]P. A. Bernhardt, J. B. Baumgardner, A. N. Bhatt, P. E. Erickson, M. F. Larsen, T. R. Pedersen, and C. L. Siefring, IEEE Trans. Plasma Sci. **39**, 2774 (2011).
[39]J. Y. N. Cho and M. C. Kelley, Rev. Geophys. **31**, 243, doi:10.1029/93RG01535 (1993).
[40]M. Galvez, S. P. Gary, C. Barnes, and D. Winske, Phys. Fluids **31**, 1554 (1988).
[41]J. D. Huba, N. T. Gladd, and K. Papadopoulos, J. Geophys. Res. **83**(A11), 5217, doi:10.1029/JA083iA11p05217 (1978).
[42]R. L. Merlino, A. Barkan, C. Thompson, and N. Dangelo, Phys. Plasmas **5**, 1607 (1998).